Upgrade of the scintillating bars detector for the ASACUSA experiment

Giovanni Costantini[1,2], *Luca* Giorleo[3], *Giulia* Gosta[1,2,*], *Marco* Leali[1,2], *Valerio* Mascagna[1,2], *Stefano* Migliorati[1,2], *Michela* Prest[4,5], *Federico* Ronchetti[4,5], *Luigi* Solazzi[3,2], *Erik* Vallazza[5], and *Luca* Venturelli[1,2]

[1]Dipartimento di Ingegneria dell'Informazione (DII), Università degli Studi di Brescia, Brescia, Italy
[2]INFN - Sezione di Pavia, Pavia, Italy
[3]Dipartimento di Ingegneria Meccanica e Industriale (DIMI), Università degli Studi di Brescia, Brescia, Italy
[4]Dipartimento di Scienze e Alta Tecnologia (DiSAT), Università degli Studi dell'Insubria, Como, Italy
[5]INFN - Sezione di Milano-Bicocca, Milano, Italy

Abstract. The upgrade of the scintillating bars detector, used in the experiments of the ASACUSA Collaboration at the CERN Antiproton Decelerator is presented. The detector consists of several modules, each one made of ≈1m long scintillating bars, which allow the detection of the charged particles produced in the annihilations of antiprotons and antihydrogens. The mechanics, the electronic readout and the data acquisition system upgrade are described.

1 Introduction

The ASACUSA collaboration (Atomic Spectroscopy And Collisions Using Slow Antiprotons) performs experiments with low energy antiprotons at the CERN Antiproton Decelerator (AD). The detector we are presenting has been used by the collaboration in different ways: to measure the antiproton annihilation cross sections on different target nuclei and energies [1–5], or by recording the annihilation rate and the vertex position of antiprotons ($\bar{p}$s) and antihydrogens ($\bar{H}$s) in the antihydrogen experimentation, where it resulted to be fundamental to demonstrate the first $\bar{H}$ production in a cusp trap [6]. The detector in the upgraded configuration will be used, in particular, in the experiment regarding the measurement of the hyperfine splitting of the ground-state (HFS-GS) of antihydrogen with the aim of performing a test of the fundamental CPT symmetry between matter and antimatter [7]. In figure 1 the experimental setup for the $\bar{H}$ production and measurement is shown.

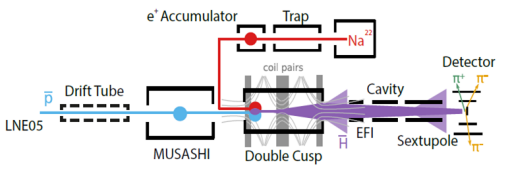

Figure 1: ASACUSA experimental setup for antihydrogen measurement.

The MUSASHI trap (see figure 1) cools and stores 100 keV antiprotons delivered by the AD with the ELENA ring (Extra Low ENergy Antiproton) [8]. Positrons, instead, are obtained from a ^{22}Na source and cooled and stored in the positron accumulator. The double-Cusp trap [9] is made by a multi-ringed electrode trap [10] housed within a magnetic field produced by a pair of superconducting coils in an anti-Helmholtz configuration [11]. Here, positrons and antiprotons mix, and the cusp magnetic field focuses, along the apparatus axis, the low-field seeking (LFS) cold ground state antihydrogen atoms. The polarised $\bar{H}$ atoms escape the trap and enter the spectrometer consisting of a microwave cavity [12, 13] to induce hyperfine transitions, followed by a state-analysing sextupole magnet that focuses the low-field seeking states and defocusses the high-field seekers. A detector records the $\bar{H}$ annihilation signal at the end of the beam-line as a function of the microwave frequency applied in the cavity [14–16]. The challenge lies in producing an intense, focused and polarised source of $\bar{H}$ atoms in the ground state. The 3D track detector, described in this work, is used to monitor the annihilations of antiproton and antihydrogen atoms.

2 Detector of antiproton annihilation

The detector consists of 8 planes made of a different number of scintillating bars (from 30 to 60), which were provided by FNAL [17]. The length and section of each bar are 96 cm and 1.5 × 1.9 cm^2 respectively. They are extruded plastic scintillators composed of Polystyrene Dow Styron 663 W + 1 % PPO + 0.03% POPOP and white TiO2 coating [18]. A hole of 2.5 mm diameter is grooved along their length to host a 1 mm diameter Y-11 type WLS fiber by Kuraray[1] glued with E30 epoxy. The emission peak of the scintillator and the absorption one of the WLS

*e-mail: giulia.gosta@unibs.it

[1]https://www.kuraray.com/

fibers, 420 nm and 430 nm respectively, are well-matched and the light output of such a system has been characterized in Ref. [18].

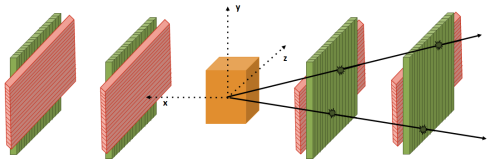

Figure 2: In a typical configuration, the detector consists of 8 planes made of a different number of scintillating bars (from 30 to 60). The planes are coupled so that the two series of bars result orthogonal and they are located around the cusp-trap in order to determine the vertex position in the 3D space.

The planes detect the charged particles crossing the scintillating bars (mostly pions emerging from antiprotons annihilations) and they are a useful tool for tuning the trap parameters during the experiment. The planes are coupled so that the two series of bars result orthogonal to give a bi-dimensional (XY) information of the particle position. The XY-modules are located around the cusp-trap as illustrated in figure 2. In this configuration, the vertex position of $\bar{p}$s and $\bar{H}$s annihilation can be determined in the 3D space.

In the past detector configuration, the light from the WLS fibers of a single plane was collected by 2 Hamamatsu[2] 64 channel H7546-B multianode PhotoMultipliers (PMTs) where only half of the available channels were used in order to reduce the cross-talk between contiguous channels. The fibers were faced to the PMTs by using aluminum plates with holes spaced in a checkboard array. The electronics readout was performed by dedicated front-end boards (FEB) equipped with a MAROC3 ASIC. The FEBs host 2 FPGAs (Altera Cyclone II), a 12 bit ADC and present a dedicated socket to connect one single PMT. The analog signals from the PMT are amplified by a pre-amplifier with a variable gain (8 bit). The signals are then fed to two different chains: the first one (analog output) consists of a slow shaper and a sample & hold circuit, the second one (digital output) is formed by a fast shaper and a discriminator.
Due to the difficulty to keep a good coupling between fibers and PMT in front of many detector movements, a loss of signal and a non-uniform efficiency were observed. Moreover, the fact that the fibers are collected in the same point and read by a single PMT caused non-natural folding of the fibers and as a consequence, the possibility of damaging the fibers. For these reasons, an upgrade was planned.

[2]https://www.hamamatsu.com/eu/en/index.html

3 DANTE: Detector for ANnihilation Tracking Experiment

3.1 Electronics

The principal upgrade regards the substitution of the PMTs with Silicon PhotoMultipliers (SiPMs), one for each fiber. The ASD RGB-SiPMs provided by AdvanSiD[3] have a 1×1 mm^2 active area completely covered with a transparent epoxy layer and they are located inside a SMD plastic package of 2.03 x 2.48 x 1.30 mm^3. The active area is composed by 625 micro-cells of 40 μm each one. The SiPMs are based on the "N-on-P" silicon technology for detection of Red, Green, and Blue light. They have a peak efficiency at 550 nm, with a detection spectrum extending from 350 nm to 900 nm. The use of the SiPMs guarantees a better coupling with the fibers and allows to have a more compact system. The SiPMs can operate in high magnetic field, they do not need high voltage and moreover the chosen model front-end readout scheme and radiation tolerance have already been tested by some members of the collaboration [19]. A better efficiency uniformity is then expected. SiPMs are mounted on new electronic boards that are then connected with the front-end boards (FEB) equipped with a MAROC3 ASIC, already in use. The advantage of this system is that these new boards can be located inside the frame and each SiPM connected with a single fiber.

3.2 Mechanical support

In the past configuration, bars were surrounded by an aluminium frame and located between two black plastic panels that hooked with the frame to create a unique and closed system. In this way, bars and fibers were not fixed in a tight way inside the frame. We improved the mechanical support, making the bars self-supporting. On the two extremities of the bars, where the fibers exit from the plastic scintillator, a pair of L-shaped aluminium extrusions were positioned one on the top and one on the bottom, tied together and hinged to the external aluminium frame. This avoids movements in the 3 directions and makes the system of the bars plus the external frame independent from the 2 black covers. A picture of the mechanical supports is shown in figure 3.

3.3 Fibers coupling

As previously described each fiber must be connected with a single SiPM that is located on the new electronic board. An accurate coupling between the 1x1 mm^2 active square area of the SiPM and the circular 1 mm diameter transmitting area of the fiber is necessary to avoid any loss of signal. Since the position of the SiPM on the board is fixed and the nominal mechanical tolerance of the black package is ±0.15 mm (both on length and width), we studied the position of the active area with respect to the housing.

[3]https://advansid.com/home

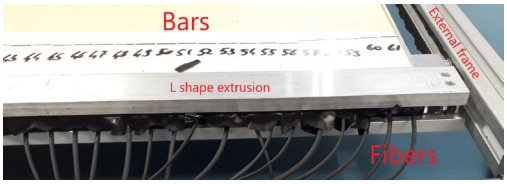

Figure 3: New mechanical support. The scintillating bars are held by 2 L-shaped aluminium extrusions tied together and hinged to the external aluminium frame, to obtain a self-supporting system.

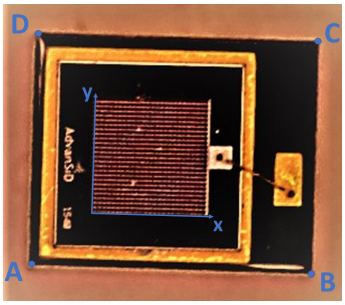

Figure 4: Picture of one SiPM. The orthogonal Cartesian system has the origin in the bottom-left vertex of the active area and the four vertices are labeled with points A,B,C,D [20].

A photo camera Canon with MACRO lens was used to take high-resolution photos of the upper surface of each SiPM. The relative position between the plastic support and the active area was obtained by analyzing the images with an online tool [20] that allows to measure distances and get points coordinates precisely once a reference system is defined. Due to the difficulty to arrange each SiPM always in the same position with respect to the camera, we identified an orthogonal Cartesian system with the origin in one of the vertices of the active area and the axes along two sides of the active square as reported in figure 4. In this way, even if the coordinate system is different for each image, our process does not depend on the possible mismatch position of the SiPMs. After the reference frame is defined, we identified the coordinates of the four vertices of the external package with respect to the axes origin as displayed in figure 4. We repeated this process for 98 SiPMs, randomly chosen, and we calculated the average values of the coordinates and their standard deviations. The results are listed in table 1. We can observe that the standard deviation is of the order of few 10^{-2} mm.

Then we focused on the planning of the fiber-SiPM coupling. We used a 3D printer to mould a coupler in resin composed by two parts: the first one that is going to be fixed on the board and the second that has to be glued to the fiber. At the end they will be connected to finalize the coupling. They were produced with the Project 2500 Pro machine (3D System, South Caroline, US) that

	$\bar{x}$ [mm]	Std. Dev x [mm]
A	−0.50	0.04
B	1.98	0.04
C	1.97	0.03
D	−0.51	0.03

	$\bar{y}$ [mm]	Std. Dev y [mm]
A	−0.52	0.02
B	−0.51	0.02
C	1.58	0.03
D	1.56	0.02

Table 1: Average values of the x and y coordinates with relative errors together with the standard deviation of the measurements for the 4 vertices of the external package for the 98 SiPMs.

Figure 5: Pictures of the two parts of the couplers, produced with the Project 2500 Pro machine that works with material jetting technology. HT250, a photocurable resin, was selected as part material, wax for support material. After the production, the parts underwent a post-process (water bath, immersion in mineral oil and ultrasonic cleaning) to eliminate the support material. The couplers before (left side) and after (right side) the water bath are shown.

works with material jetting technology; this technology is an inkjet printing process that uses piezo printhead technology to deposit photocurable plastic resin droplets layer by layer. HT250, a photocurable resin provided by 3D System, was selected as the part material, while wax for the support material. After the production, the parts underwent a post process (water bath, immersion in mineral oil and ultrasonic cleaning) to eliminate the support material. In figure 5 the couplers before (left side) and after (right side) the water bath are shown.

The component secured on the board is created with a rectangular hole where the SiPM can be housed. In order to know the correct dimension of the rectangle, we used the data obtained from the position of the vertex to determine the lengths of the 4 sides. The result of the analysis on 98 SiPMs, shows that the average values are always compatible with the nominal ones within the mechanical tolerance, even if the average values for the two short sides (BC and DA) are 3% higher than the nominal lengths. This

analysis has allowed us to produce the couplers with the correct dimension for housing the SiPMs.

The other component, the one that is fixed to the fiber, consists in a cylinder where the fiber is stringed. The coupling of the two components with the board is illustrated in figure 6.

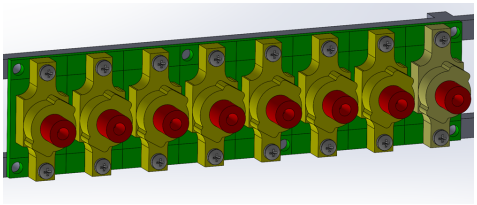

Figure 6: 3D scheme of the coupling between the two resin couplers (the ocher and the red parts) and the electronic board (green part) on which the SiPMs are fixed.

All the fibers were cut, inserted in the cylinders, glued with epoxy and then polished. In figure 7 the couplers with the housing for the SiPMs, fixed to the board and the ones coupled with the fibers are shown. At this point, the cylinders are inserted in the board component and the fibers and the SiPMs are coupled.

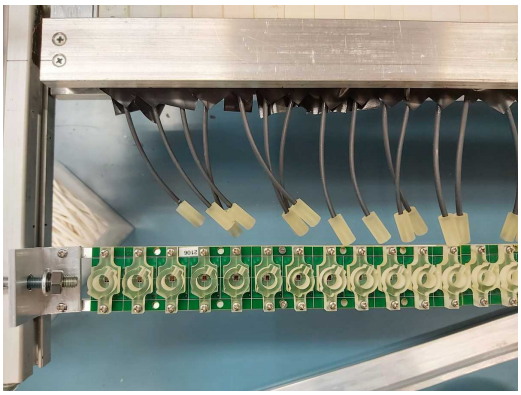

Figure 7: Pictures of the couplers. The first component with the housing for the SiPMs is fixed to the board and the second one is glued with fibers. The cylinders must be slotted in the board component and the fibers and the SiPMs can be coupled.

4 Preliminary test

Preliminary measurements are now in progress with cosmic-rays. As shown in the upper part of figure 8, two plastic scintillators and two silicon microstrip XY detectors are located under one of the plane of the scintillating bars. The coincidence between the two scintillators provides the trigger for the data acquisition system and the microstrip detectors are used to track the cosmic rays. Extrapolating the hit position of each track on the bars plane and recording their signals it is possible to characterize each channel in terms of detection efficiency and uniformity of the light yield. Many weeks of data taking are needed to collect enough statistic and the analysis is still in progress. Nevertheless, the already acquired data (e.g. the hit profile of one plane is shown in the lower part of figure 8) give a feedback on the uniformity of the optical fibers-SiPM coupling and small interventions to correct defects are in progress.

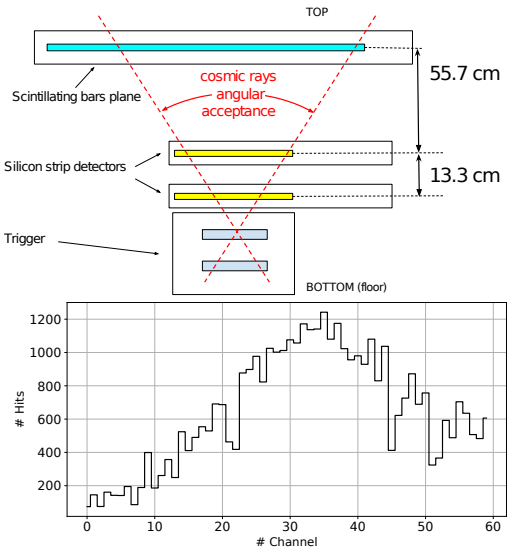

Figure 8: Upper part: the experimental setup for cosmic data taking campaign where a scintillating bar plane is put under test thanks to two plastic scintillators and two silicon microstrip detectors as a reference. Lower part: a hit profile of the cosmic rays on one plane. The plot shape is determined by the angular distribution of the cosmic rays and the geometrical acceptance of the trigger detectors, whereas local non uniformities are presumably due to bad fiber-SiPM couplings or a mechanical pull of the electronic board hosting the SiPMs. In both cases, they could be corrected by simple mechanical adjustments.

5 Conclusion

The upgrade of the scintillating bars detectors for the ASACUSA experiment has been presented. It mainly consists in the replacement of PhotoMultiplier tubes with Silicon PhotoMultipliers, that allow a better coupling with fibers and better performances in high magnetic field. The mechanical support has been modified to make the bars self-supported and resin couplers have been designed and produced for connecting a fiber with a SiPM. Performance and efficiency tests are now in progress.

References

[1] H. Aghai-Khozani, A. Bianconi, M. Corradini, R. Hayano, M. Hori, M. Leali, E. Lodi Rizzini, V. Mascagna, Y. Murakami, M. Prest et al., Nuclear Physics A **970**, 366 (2018)

[2] K. Todoroki, D. Barna, R. Hayano, H. Aghai-Khozani, A. Sótér, M. Corradini, M. Leali, E. Lodi-Rizzini, V. Mascagna, L. Venturelli et al., Nuclear Instruments and Methods in Physics Research Section A: Accelerators, Spectrometers, Detectors and Associated Equipment **835**, 110 (2016)

[3] H. Aghai-Khozani, D. Barna, M. Corradini, R. Hayano, M. Hori, T. Kobayashi, M. Leali, E. Lodi-Rizzini, V. Mascagna, M. Prest et al., The European Physical Journal Plus **127**, 125 (2012)

[4] H. Aghai-Khozani, D. Barna, M. Corradini, D. De Salvador, R. Hayano, M. Hori, T. Kobayashi, M. Leali, E. Lodi-Rizzini, V. Mascagna et al., Hyperfine Interactions **234**, 85 (2015)

[5] H. Aghai-Khozani, D. Barna, M. Corradini, D. De Salvador, R. Hayano, M. Hori, M. Leali, E. Lodi-Rizzini, V. Mascagna, M. Prest et al., Nuclear Physics A **1009**, 122170 (2021)

[6] Y. Enomoto, N. Kuroda, K. Michishio, C.H. Kim, H. Higaki, Y. Nagata, Y. Kanai, H.A. Torii, M. Corradini, M. Leali et al., Phys. Rev. Lett. **105**, 243401 (2010)

[7] C. Malbrunot, C. Amsler, S. Arguedas Cuendis, H. Breuker, P. Dupre, M. Fleck, H. Higaki, Y. Kanai, B. Kolbinger, N. Kuroda et al., Philosophical Transactions of the Royal Society A: Mathematical, Physical and Engineering Sciences **376**, 20170273 (2018)

[8] V. Chohan, C. Alanzeau, M.E. Angoletta, J. Baillie, D. Barna, W. Bartmann, P. Belochitskii, J. Borburgh, H. Breuker, F. Butin et al., *Extra Low ENergy Antiproton (ELENA) ring and its Transfer Lines: Design Report*, CERN Yellow Reports: Monographs (CERN, Geneva, 2014), `https://cds.cern.ch/record/1694484`

[9] Y. Nagata, N. Kuroda, P. Dupre, B. Radics, M. Tajima, A.A. Capon, M. Diermaier, C. Kaga, B. Kolbinger, M. Leali et al., Proceedings of the 12th International Conference on Low Energy Antiproton Physics (LEAP2016) (2017)

[10] A. Mohri, H. Higaki, H. Tanaka, Y. Yamazawa, M. Aoyagi, T. Yuyama, T. Michishita, Japanese Journal of Applied Physics **37**, 664 (1998)

[11] C. Sauerzopf, A.A. Capon, M. Diermaier, P. Dupré, Y. Higashi, C. Kaga, B. Kolbinger, M. Leali, S. Lehner, E.L. Rizzini et al., Hyperfine Interactions **237**, 103 (2016)

[12] N. Kuroda, S. Ulmer, D.J. Murtagh, S.V. Gorp, Y. Nagata, M. Diermaier, S. Federmann, C.M. M. Leali, V.Mascagna, O. Massiczek et al., Nature Communications **5**, 3089 (2014)

[13] C. Malbrunot, M. Diermaier, M. Simon, C. Amsler, S. Arguedas Cuendis, H. Breuker, C. Evans, M. Fleck, B. Kolbinger, A. Lanz et al., Nuclear Instruments and Methods in Physics Research Section A: Accelerators, Spectrometers, Detectors and Associated Equipment **935**, 110 (2019)

[14] E. Widmann, C. Amsler, S. Arguedas Cuendis, H. Breuker, M. Diermaier, P. Dupré, C. Evans, M. Fleck, A. Gligorova, H. Higaki et al., Hyperfine Interactions **240**, 5 (2018)

[15] Y. Nagata, N. Kuroda, M. Ohtsuka, M. Leali, E. Lodi-Rizzini, V. Mascagna, M. Tajima, H. Torii, N. Zurlo, Y. Matsuda et al., Nuclear Instruments and Methods in Physics Research Section A: Accelerators, Spectrometers, Detectors and Associated Equipment **840**, 153 (2016)

[16] B. Kolbinger, C. Amsler, H. Breuker, M. Diermaier, P. Dupré, M. Fleck, A. Gligorova, H. Higaki, Y. Kanai, T. Kobayashi et al., EPJ Web of Conferences **181** (2018)

[17] A. Pla-Dalmau, A.D. Bross, K.L. Mellott, Nuclear Instruments and Methods in Physics Research Section A: Accelerators, Spectrometers, Detectors and Associated Equipment **466**, 482 (2001)

[18] M. Corradini, M. Leali, E. Lodi-Rizzini, V. Mascagna, V. Prest, L. Vallazza, L. Venturelli, Hyperfine Interactions **233**, 53 (2015)

[19] F. Acerbi, G. Ballerini, A. Berra, C. Brizzolari, G. Brunetti, M. Catanesi, S. Cecchini, F. Cindolo, A. Coffani, G. Collazuol et al., Journal of Instrumentation **14**, P02029 (2019)

[20] A. Rohatgi, *Webplotdigitizer: Version 4.5* (2021), `https://automeris.io/WebPlotDigitizer`